International Journal of Applied Pharmaceutics

ISSN- 0975-7058 Vol 16, Special Issue 1, 2024

Original Article

INCREASED DISSOLUTION RATE OF ACECLOFENAC BY FORMATION OF MULTICOMPONENT CRYSTALS WITH L-GLUTAMINE

ADHITYA JESSICA[1], SIRLY WAHYUNI N. YASA[2], ERIZAL ZAINI[1], LILI FITRIANI[1*]

[1]Department of Pharmaceutics. Faculty of Pharmacy. Universitas Andalas. Padang-25163. Indonesia. [2]Bachelor Program. Faculty of Pharmacy. Universitas Andalas. Padang-25163. Indonesia

*Corresponding author: Lili Fitriani; *Email: lilifitriani@phar.unand.ac.id

Received: 17 Oct 2023, Revised and Accepted: 23 Nov 2023

ABSTRACT

Objective: The objectives of this research were to improve the solubility as well as the rate of dissolution of aceclofenac (ACF) through the formation of multicomponent crystals (MCC) with L-glutamine (LGLN) as a coformer and following the liquid-assisted grinding (LAG) technique.

Methods: MCC of ACF and LGLN was formed by Liquid Assisted Grinding (LAG) technique. Powder X-ray Diffractometer (PXRD), Differential Scanning Calorimeter (DSC), Fourier Transform Infrared (FT-IR) spectrometer, Particle Size Analyzer (PSA), and Scanning Electron Microscope (SEM) were used for MCC characterization. Solubility and dissolution test were determined using ultraviolet-visible (Uv-Vis(spectrophotometer.

Results: The results showed a decrease in the diffraction peak intensity, melting point, and enthalpy of fusion. FT-IR analysis showed a non-significant wavenumber shift compared to intact components. These characterizations showed that MCC formed a eutectic mixture. SEM and particle size analysis showed a homogeneous particle rod shape and decreased particle size. ACF's solubility in MCC increased 2.21 times more than intact form. MCC's dissolution rate increased by 5.34 times and 5.56 times, respectively, after 60 min in phosphate buffer pH 6.8 and CO2-free distilled water.

Conclusion: The formation of MCC of ACF and LGLN considerably enhances ACF's solubility and dissolution rate.

Keywords: Aceclofenac, L-glutamine, Multicomponent crystal, Eutectic mixture, Solubility, Dissolution rate

DOI: https://dx.doi.org/10.22159/ijap.2024.v16s1.09 Journal homepage: https://innovareacademics.in/journals/index.php/ijap

INTRODUCTION

Aceclofenac (ACF) is a nonsteroidal anti-inflammatory drug (NSAID) with anti-inflammatory, analgesic, and antipyretic pharmacological activities which has been used in acute-chronic bone and muscle diseases treatment including osteoarthritis, ankylosis spondylitis, rheumatoid arthritis, and back pain. ACF's action mechanism is selectively inhibiting cyclooxygenase 2 (COX-2) enzymes. The selectivity of ACF towards COX-2 over COX-1 makes it better tolerated than other NSAIDs such as diclofenac, naproxen, piroxicam, indomethacin, and ketoprofen. Due to its safety, ACF is an NSAID option for long-term therapy [1, 2]. Based on the Biopharmaceutical Classification System (BCS), ACF belongs to class II, with high permeability and low solubility in water (58 µg/ml) [3]. The low solubility of ACF results in its low bioavailability in the oral administration route. Therefore, modification of the solubility and dissolution of ACF in its oral dosage form is essential to improve its bioavailability and efficacy [4].

Modifications to improve the solubility of ACF through the formation of inclusion complexes and solid dispersion systems have already been carried out. ACF inclusion complex with β-cyclodextrin by the kneading method showed an increase in the *in vitro* dissolution rate by 13.72 times compared to intact ACF in 60 min. Solid dispersion of ACF with poloxamer 407 increased its solubility by 12.5 times and dissolution rate in 30 min by 3.75 times. However, solid dispersion systems have several disadvantages, including physical stability and sensitivity to temperature and humidity. As a result, solid dispersion systems may change crystallinity properties and decrease the dissolution rate [5]. Cyclodextrins (CDs) used in inclusion complex systems are practically nontoxic. However, higher doses of CDs may harm the kidneys [6]. Another alternative way that has been done to improve the solubility of ACF is to form a multicomponent crystal (MCC). Drugs' physicochemical features, such as water solubility, dissolved level, and stability, are successfully strengthened by preparing multicomponent crystals without altering their pharmacological action [7].

MCCs are broadly categorized into cocrystals, salts, and solvates/hydrates [7]. Cocrystals combine two neutral molecules or ions at specific stoichiometric ratios with non-covalent interactions such as hydrogen, Van der Waals, or π-π bonds. Cocrystal consists of one active pharmaceutical ingredient (API) and a crystal-forming pair known as a coformer. Cocrystals are similar to salts; the difference lies in the presence or absence of proton transfer between API and coformers. The transfer of protons between acid-base pairs occurs at the time of salt formation, while it is not at the appearance of cocrystals. At ambient temperature, the physical characteristics of cocrystals and solvates are distinct. Solvates are liquid, while cocrystals are solid. Solvates containing water are called hydrate [8-11].

Coformers must be classified as generally recognized as safe (GRAS), which are ingredients categorized as safe by the Food and Drug Administration (FDA) for human consumption [12]. MCCs of ACF have been prepared with several coformers before, such as urea, dimethyl urea, lysine, L-cystine, nicotinamide, nicotinic acid, gallic acid, chitosan, and caffeine [13-16].

This study selects L-glutamine (LGLN) as a coformer to form an MCC with ACF. LGLN is declared a safe additive that is on the FDA's GRAS list and predicted to be able to form cocrystals or salts with ACF based on theΔpKa value ([pKa (base) −pKa (acid)]). If ΔpKa of API and coformer≥ 3, it will likely form a salt, while if ΔpKa <3, it will have the potential to develop a cocrystal. ACF (pKa = 4.7) and LGLN (pKa1=2.17 and pKa2=9.13) haveΔpKa 2.53 and 4.43 [17]. Synthon engineering can also predict the formation of cocrystals; LGLN has carboxyl and amide groups, while ACF has carboxyl and hydroxyl groups acting as donors or receptors to form hydrogen bonds [18, 19]. In addition, LGLN, as a coformer, can form cocrystals with several other APIs [20]. LGLN is also proven to reduce the side effects of flatulence from mesalamine, one of the NSAIDs, by stabilizing acid bases in the digestive tract [18, 21]. Recent research shows that LGLN can have a good effect on the health of the digestive tract by maintaining the balance of the gut microbiome and the

integrity of the walls of the intestinal mucosa, as well as modulating the inflammatory response in the digestive tract [23].

The formation of MCC of ACF-LGLN is carried out using the Liquid-Assisted Grinding (LAG) method, which is an effective method suitable for preparing MCC [10]. The physicochemical properties of MCC are then characterized with Powder X-ray Diffractor (PXRD), Differential Scanning Calorimeter (DSC), Fourier Transform Infrared (FT-IR) spectrometer, Particle Size Analyzer (PSA), Scanning Electron Microscope (SEM), as well as solubility and dissolution rate tests.

MATERIALS AND METHODS

Materials

ACF (BOC science, the USA), LGLN (Tokyo Chemical Industry, Japan), ethanol pro analysis (Merck, Germany), potassium dihydrogen phosphate (Merck, Germany), and distilled water.

Methods

Formation of physical mixtures and MCC

A physical mixture of ACF-LGLN was prepared at a mol ratio of 1:1. ACF was weighed at 0.354 g and LGLN at 0.146 g, respectively, and then mixed homogeneously. The MCC was prepared in the same amount as the physical mixture, and then the mixture was ground for 10 min while adding ~3 drops of ethanol. Both samples were then stored in a tightly closed container and placed in a desiccator.

DSC analysis

4 mg of each sample was placed on a closed aluminum plate. DSC (SETARAM type EVO-131, Lyon, France) instrument was then programmed at 25–200 °C temperature range and heating rate at 10 °C/min. The analysis was performed on the ACF, LGLN, physical mixture, and MCC of ACF-LGLN.

PXRD analysis

The sample was analyzed by X-ray diffraction using a diffractometer (XPERT-PRO type PAN, Netherlands) under the following measurement conditions: Cu metal target, K filter, 40 kV voltage, 30 mA current, 2 5–50 ° range. The ACF, LGLN, physical mixture and MCC of ACF-LGLN underwent analysis.

FT-IR analysis

FT-IR analysis (Perkin Elmer FT-IR, USA) was performed by placing the sample on top of the ATR crystal until it covered all the crystal surfaces. Then, the sample was closed by applying pressure, and absorption spectrum retrieval was performed against the sample. The analysis was performed for the ACF, LGLN, physical mixture, and MCC of ACF-LGLN.

SEM analysis

A gold/palladium coating was applied to the powder sample and placed on an aluminum sample holder. The powder sample was then examined using several SEM magnifications (FlexSEM1000, Japan). 20 kV of voltage and 12 mA of current were the settings. The ACF, LGLN, physical mixture and MCC of ACF-LGLN underwent analysis.

Particle size analysis

Particle size analysis was carried out with a particle size analyzer (PSA, Shimadzu SALD-2300) with the principle of dynamic light scattering (DLS). The study was performed on intact ACF, a physical mixture, and MCC of ACF-LGLN. Before measurement, each sample was dispersed in 5 ml of distilled water, put into the sample holder of the particle size analyzer, and analyzed at a temperature of 25 °C.

Solubility test

Excessive amounts of each ACF, physical mixture, and MCC of ACF-LGLN were added in 100 ml CO2-free distilled and the was kept in an orbital shaker for solubility test at room temperature overnight. The solution was then filtered using a Whatman filter with a 0.45 m pore size, and the filtrate was then subjected to three independent analyses using Ultraviolet-Visible (UV-Vis) spectrophotometry (Shimadzu type UV-1280, Japan) at 274.8 nm. A one-way ANOVA test was used for statistical analysis of the solubility data.

Dissolution profile

The dissolution profile was carried out with a USP type 2 dissolution apparatus (Hanson SR8PLUS, USA) with a stirring speed of 50 rpm at 37±0.5 °C. The dissolution flask was filled with a 900 ml dissolution medium: phosphate buffer pH 6.8 and CO_2-free distilled water. Each media added 0.1% sodium lauryl sulfate (SLS) as a surfactant to increase the wettability of the sample [24]. Samples were weighed equal to 100 mg of ACF and then put into the dissolution flask. The amount of ACF dissolved was determined on the 5th, 10th, 15th, 30th, 45th, and 60th minutes using UV-Vis spectrophotometry (Shimadzu UV-1280, Japan) at λmax 272.8 nm for phosphate buffer and 274.8 nm for distilled water respectively. The dissolution test was performed for intact ACF, physical mixture, and MCC triplicated. The dissolution data was analyzed statistically using a two-way ANOVA test.

RESULTS AND DISCUSSION

DSC analysis

Analysis of DSC can be used as a simple preliminary screening of MCC formation. MCC is formed when a new solid phase appears in which the DSC analysis of the test sample will have a different melting point with its intact compound [25].

The thermogram (fig. 1) shows that the physical mixture and MCC have one sharp endothermic peak, which means ACF and LGLN fuse simultaneously. Several small endothermic peaks above the sample's melting point indicate the sample's degradation in the physical mixture and MCC thermograms [26–28].

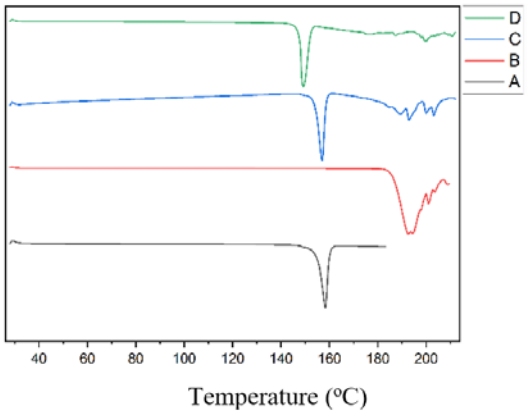

Fig. 1: Overlayed thermogram of (A) ACF (B) LGLN (C) physical mixture of ACF-LGLN (D) MCC of ACF-LGLN (1:1)

Based on thermograms, the physical mixture and MCC of ACF-LGLN show the characteristics of eutectic mixtures since they have one single endothermic peak and a lower melting point than their constituent components' melting point [29]. A decrease in melting point of the physical mixture (153.52 °C) and MCC (149.21 °C) is in between intact ACF (154.77 °C) and LGLN (192.29 °C). One endothermic peak with a melting point lower than its pure component was also detected in the DSC data of ACF and caffeine eutectic mixtures [30]. Due to a cohesive force that causes weak contacts and the creation of irregular heterogeneous crystalline arrangements of the active substance and the coformer, the melting point of the eutectic mixture decreases [29].

Moreover, there is also a decrease in the enthalpy value, which indicates a reduction in the amount of energy needed to melt substances related to the decline in the degree of crystallinity of the physical mixture and the MCC [31]. Furthermore, confirmation of the formation of eutectic combinations and a decrease in the degree of crystallinity will be proven by the analysis using X-ray diffraction.

XRD analysis

X-ray diffraction (XRD) is one of the nondestructive techniques for characterizing crystals. It can be used to observe the presence or

absence of different new peaks on MCC compared to intact components. XRD analysis can also be used to determine the crystallinity of a compound [32, 33]. The data from the XRD analysis and peak values at position 2θ of each sample can be seen in fig. 2 and table 1.

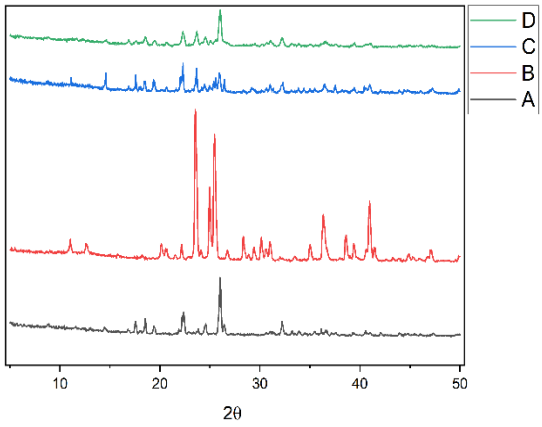

Fig. 2: Diffractogram of (A) ACF, (B) LGLN, (C) Physical mixture of ACF-LGLN, and (D) MCC of ACF-LGLN (1:1)

02

The X-ray diffractogram's distinctive and sharp peaks indicate that the four samples are in the crystalline phase [33]. The specific peak data of each sample at position two are presented in table 1. ACF has specific peaks at 18.5331°, 22.3811°, 25.9951°, and 32.2091°, while LGLN at 23.5251°, 24.9811°, 25.9951°, and 39.385°. In addition, there is no new peak in the physical mixture or MCC. This result suggests that no new crystalline phase is formed. The XRD analysis data support the DSC analysis result, which shows that the MCC formed combines ACF and LGLN or a eutectic mixture. The formation of eutectic mixtures occurs due to the distribution of molecules of one crystal into the crystal structure lattice of other components. Therefore, in the results of the XRD analysis, there is only a slight difference between the diffraction pattern of the eutectic mixture and the pure constituent components [29].

Table 1 shows that MCC (1:1) has a lower diffractogram peak intensity than its physical mixture. This finding indicates a decrease in the degree of crystallinity, which may be caused by a small fraction of amorphous material obtained in the MCC samples due to the grinding process with the LAG method [33, 34].

FT-IR analysis

FT-IR analysis was performed to identify functional groups from ACF and LGLN and to see the intermolecular interactions of the physical mixture and MCC. The IR spectrum and wave number data of each sample can be seen in fig. 3 and table 2.

Table 1: Specific peak intensity of ACF, LGLN, physical mixture of ACF-LGLN, and MCC of ACF-LGLN

2nd place θ	Peak intensity			
	ACF	LGLN	Physical mixture	MCC
18.5331	414.991	-	331.680	257.804
22.3811	528.990	-	675.775	373.370
23.5251	-	3037.407	265.837	224.548
24.9811	-	1522.556	206.996	175.038
25.4491	-	2552.263	239.001	176.800
25.9951	1208.378	132,03	460.562	772.576
32.2091	354.653	564.0069	307.202	256.467
39.3851	-	1873.651	208.583	156.019

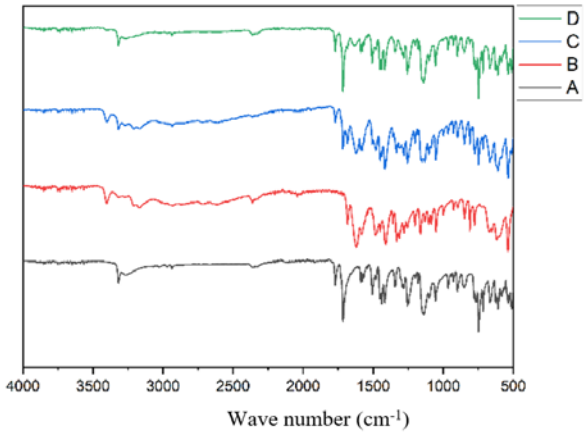

Fig. 3: FT-IR spectrum of (a) ACF; (b) LGLN; (c) physical mixture of ACF-LGLN; and (d) MCC of ACF-LGLN

Table 2 shows data from FT-IR analysis of ACF, LGLN, physical mixture of ACF-LGLN, and MCC of ACF-LGLN. ACF has a typical absorption at wave numbers 3317.56, 3263.56, and 1714.72 cm^{-1}, sequentially indicating the presence of N-H, O-H, and C=O bonds in the ACF structure. In LGLN, a typical absorption suggests a bond between the atoms N-H, O-H, and C=O at wave numbers 3404.36, 3165.19, and 1683.86 cm^{-1}.

Table 2: Wave numbers comparison of ACF, LGLN, physical mixture of ACF-LGLN, and MCC of ACF-LGLN

Functional groups	Wave number range (cm^{-1})	Wave number (cm^{-1})			
		ACF	LGLN	Physical mixture	MCC
N-H	3500-3300	3317.56	3404.36	3319.49	3317.56
O-H	3300-2500	3263.56	3165.19	3207.62	3267.41
C=O	1900-1650	1714.72	1683.86	1716.65	1716.65

The FT-IR analysis of the physical mixture and MCC showed characteristics of the eutectic mixture. There was no significant difference in the results of the FT-IR analysis of the physical mixture and MCC compared to its pure constituent. The physical mixture absorbs at wave numbers 3319.49, 3207, 62, and 1716.65 cm^{-1}, while the MCC absorbs at 3317.56, 3267.41, and 1716.65 cm^{-1}. In eutectic mixtures, no intermolecular interactions will be found. There are only weak intermolecular bonds between the constituent components, which are dominated by cohesive forces between molecules. Meanwhile, if there is a significant shift in the number of waves in the MCC, it indicates a strong interaction that indicates the formation of cocrystals or salts [29]. Therefore, the FT-IR results of eutectic mixtures will generally show the same wave number as the pure constituent or only a slight difference in the spectrum due to weak hydrogen bonds that are likely to form, for example, in the case of the formation of eutectic mixtures of nicotinamide and nimesulide [29, 35].

SEM analysis

Morphology and particle size will affect the physical properties of the crystal [36]. SEM observations aim to visually compare the MCC formed with the intact compound [37]. Fig. 4 shows SEM images of ACF, LGLN, a physical mixture, and a MCC. It can be seen that there are noticeable morphological differences in each sample. ACF is irregularly polyhedral, while LGLN has a long rod shape. The morphological image of the physical mixture is combination morphology of ACF and LGLN. The morphology and particle size of the eutectic mixture will be affected by the manufacturing method used. SEM images of MCC show a smaller particle size and a more homogeneous particle shape, which is the result obtained due to the influence of the energy given to the sample during the grinding process with the LAG method [38].

Particle size analysis with particle size analyzer (PSA)

PSA analysis was performed to determine the sample's average particle size and distribution [39]. The PSA analysis data of intact ACF, physical mixture, and MCC can be seen in table 3 and fig. 5.

The average particle size in ACF, physical mixture, and MCC were 54.365±0.266, 54.568±0.265, and 2.974±0.422 μm, respectively. This result followed the SEM analysis results, in which the morphology of MCC morphologically showed a smaller particle size. In addition, the analysis results with PSA also obtained a bell-shaped particle size distribution graph, indicating that the particle size was homogeneously distributed [40].

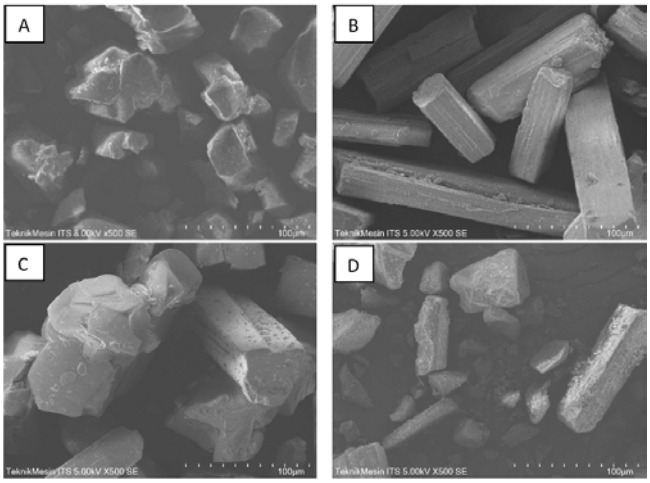

Fig. 4: SEM morphology images of compounds at a magnification of 500x (A) ACF; (B) LGLN; (C) physical mixture of ACF-LGLN; and (D) MCC of ACF-LGLN

Table 3: Particle size analysis data

Sample	Average particle size (μm)
ACF	54.365±0.266
Physical mixture	54.568±0.265
MCC	2.974±0.422

N=3, data are given in mean±SD

Solubility test

The average amount of dissolved ACF in CO_2-free distilled water from the experiments was obtained at 5.821±0.052 mg/100 ml. The solubility result of ACF in water obtained is close to the data in the literature, which is 58 mg/ml (5.8 mg/100 ml) [3]. The increase in the solubility rate can be seen from the data in table 4. Both the solubility of the physical mixture increased significantly by 2.04 times and the MCC by 2.21 times.

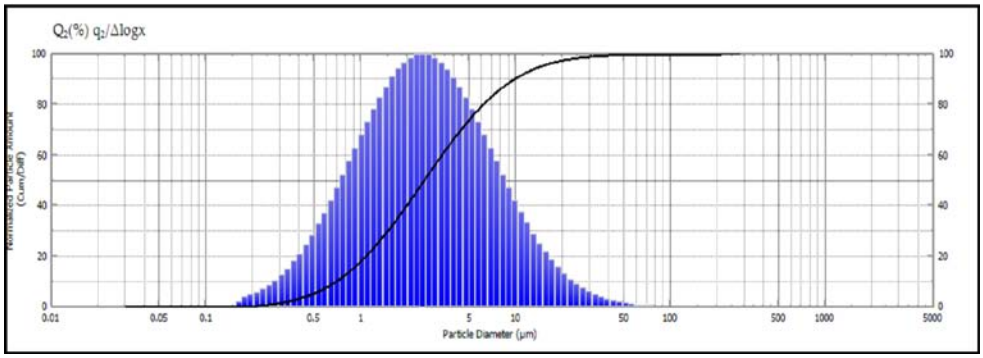

Fig. 5: Particle size distribution graph of MCC

Table 4: ACF solubility test results

Sample	Average levels of dissolved ACF±(SD) (mg/100 ml)	Solubility enhancement
ACF	5.821±0.052	-
Physical mixture	11.891±0.102	2.04 times
MCC	12.876±0.102	2.21 times

N=3

The increase in the solubility of the physical mixture and MCC compared to intact ACF is supported by previous characterization results regarding the formation of eutectic mixtures. A decrease in melting point and melting enthalpy, as well as a reduction of the degree of crystallinity and energy of crystalline bonds, impact the enhancement of eutectic mixture solubility. Although both SEM and PSA analysis showed a decrease in particle size, in this study, the particle size reduction did not have a significant relationship with the increase in solubility. The PSA results showed a decrease in the size of the MCC particle by 18.28 times of intact ACF, while the solubility only increased by 2.21 times. Thus, the increase in solubility likely occurred due to the formation of a eutectic mixture of ACF with LGLN, which has a coformer and is very quickly soluble in water. LGLN is likely to act as a hydrophilic carrier that helps increase the solubility of ACF [29].

Dissolution rate

ACF is hydrophobic and has low solubility and wettability in water, which causes floating on the surface of the dissolution medium and inhibits the contact of the medium with the substance, which may interfere with the dissolution test process. Therefore, 0.1% of SLS was added to the dissolution medium, which acts as a surfactant to increase the wettability of the substance.

The dissolution in CO_2-free distilled water showed a correlation of an increase in ACF released equal to the rise in ACF solubility in CO_2-free distilled water, where the amount of ACF dissolved in the MCC was more remarkable than the physical mixture. The average percentage of ACF dissolved in distilled water medium after 60 min was 10.850%, 11.076%, and 57.939% for intact ACF, physical mixture, and MCC, respectively (table 5). A graph of the increase in the dissolution rate in the CO_2-free distilled water medium can be seen in fig. 6. The increase in dissolution of the physical mixture and MCC were 1.020 times and 5.340 times compared to intact ACF.

The dissolution test was also carried out on the pH 6.8 phosphate buffer medium to represent ACF release under *in vivo* conditions. ACF is a weakly acidic drug that will be ionized and soluble in an alkaline environment. Generally, weakly acidic drugs will be absorbed in the intestines. The dissolution test using a pH 6.8 phosphate buffer medium after 60 min for intact ACF, physical mixture, and MCC were 8.428 %, 9.508 %, and 46.853 %, respectively (table 6). A graph of the increase in the dissolution rate in the pH 6.8 phosphate buffer medium can be seen in fig. 7. The increased dissolution of the physical mixture and MCC were 1.128 times and 5.559 times compared to ACF.

Table 5: Dissolution rate of ACF in CO02$_2$-free distilled water medium

Time (min)	% Of average dissolution		
	ACF	Physical mixture	MCC
0	0	0	0
5	8.057 ± 0.529	8.264 ± 0.156	51.342 ± 0.957
10	8.382 ± 0.395	8.640 ± 0.148	52.880 ± 1.197
15	8.630 ± 0.395	8.914 ± 0.187	54.608 ± 1.080
30	9.442 ± 0.489	9.660 ± 0.250	55.947 ± 1.617
45	10.129 ± 0.536	10.311 ± 0.247	57.322 ± 1.458
60	10.850 ± 0.585	11.076 ± 0.182	57.939 ± 1.193

N=3, data are given in mean±SD

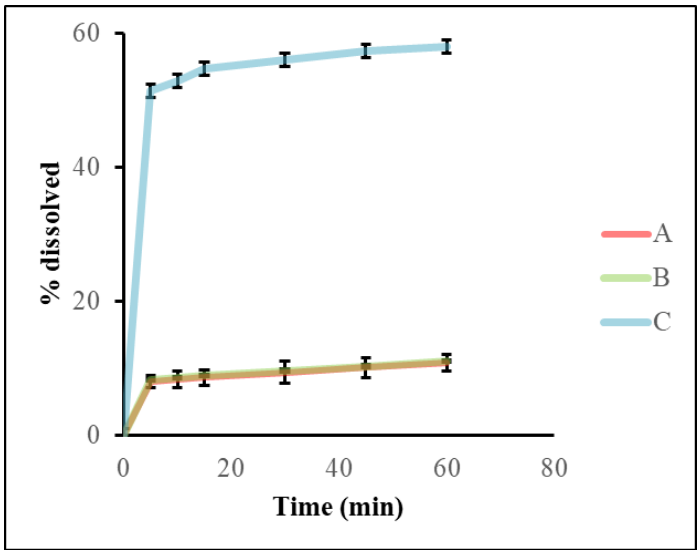

Fig. 6: Dissolution rate in CO03$_2$-free distilled water medium (A) ACF, (B) physical mixture, and (C) MCC. Error bars indicate standard deviation of 3 determination

Table 6: Dissolution rate of ACF in phosphate buffer medium pH

Time (min)	% Of average dissolution		
	ACF	Physical mixture	MCC
0	0	0	0
5	3.398 ± 0.459	4.578 ± 0.208	38.090 ± 0.964
10	4.057 ± 0.262	5.763 ± 0.070	40.702 ± 1.262
15	4.719 ± 0.265	6.345 ± 0.078	42.977 ± 0.832
30	5.935 ± 0.288	7.640 ± 0.728	44.113 ± 0.947
45	7.318 ± 0.391	8.462 ± 0.999	45.654 ± 1.076
60	8.428 ± 0.510	9.508 ± 1.394	46.853 ± 0.708

N=3, data are given in mean±SD

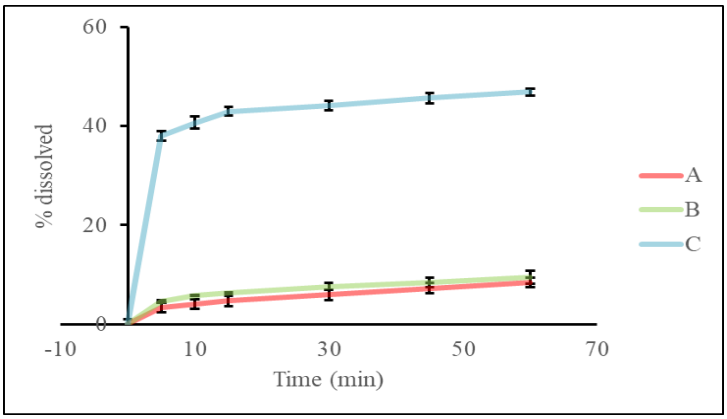

Fig. 7: ACF dissolution in medium phosphate buffer pH 6.8 (A) ACF, (B) physical mixture of ACF-LGLN, and (C) MCC of ACF-LGLN. Error bars indicate standard deviation of 3 determination

Based on the test results, the ACF dissolution was higher in CO_2-free distilled water medium than phosphate buffer pH 6.8 with an additional 0.1% SLS. This result is anticipated due to the different factors of the dissolution medium used. The addition of SLS to the dissolution medium is likely to affect the increase in pH of the CO_2-free distilled water medium because SLS has a pH range from 7 to 9.5 [41]. A large pH in a weakly acidic ACF will increase solubility, accelerating the dissolution rate. In the phosphate buffer pH 6.8 medium, the addition of SLS will likely not affect the medium's pH due to the buffer's properties, which can maintain pH despite adding a small amount of acid or base.

The increase in the dissolution in the physical mixture and MCC is due to the interaction between the two components of the substance, forming a conglomeration. The conglomeration of substances that causes a decrease in the melting point and enthalpy of melting substances can be seen from the results of the DSC analysis. A decrease in the melting point and melting enthalpy indicates a reduction in the degree of crystallinity of the physical mixture and the MCC compared to intact ACF [29]. In the data from the XRD analysis, a lower peak of the physical mixture and MCC diffractogram was obtained compared to pure ACF, which indicates a decrease in the degree of crystallinity [33].

The increase in the dissolution rate in MCC is also supported by PSA data, showing a smaller particle size of MCC than its intact substances. A decrease in particle size will increase the contact surface area of the substance and improve the wettability of the sample so that the substance is easier to disperse inside the medium [29].

Intact ACF and physical mixtures did not differ significantly ($p>0.05$), while intact ACF physical mixture differed statistically from MCC. The relationship of the dissolution with the type of medium used was also tested, in which the p-value is<0.05, and it was concluded that the type of medium used influences the dissolution rate of ACF, physical mixture, and MCC.

CONCLUSION

LGLN can be used as a coformer to form MCC with ACF, proven by characterization results with DSC, PXRD, and FT-IR, indicating the formation of eutectic mixtures. MCC formation of ACF-LGLN increases the solubility of ACF by 2.21 times, and the dissolution of ACF after 60 min in phosphate buffer pH 6.8 medium and CO_2-free distilled were 5.56 times and 5.34 times higher statistically than water intact ACF.

FUNDING

The LPPM Universitas Andalas RPT scheme funded the research with grant number T/1/UN16.19/PT.01.03/KO-RPT/2023.

AUTHORS CONTRIBUTIONS

Concept: LF, EZ, AJ, Design: LF, EZ, AJ, SWNY, Data Collection or Processing: SWNY, LF, AJ, Analysis or Interpretation: SWNY, LF, AJ, Literature Search: SWNY, LF, AJ, Writing: SWNY, LF, AJ, EZ.

CONFLICT OF INTERESTS

The authors declare no conflict of interest with the data contained in the manuscript.

REFERENCES

1. Iolascon G, Gimenez S, Mogyorosi D. A review of aceclofenac: analgesic and anti-inflammatory effects on musculoskeletal disorders. J Pain Res. 2021;14:3651-63. doi: 10.2147/JPR.S326101, PMID 34876850.
2. Sipos E, Kosa N, Kazsoki A, Szabo ZI, Zelko R. Formulation and characterization of aceclofenac-loaded nanofiber based orally dissolving webs. Pharmaceutics. 2019;11(8):417. doi: 10.3390/pharmaceutics11080417, PMID 31426548.
3. Goud NR, Suresh K, Nangia A. Solubility and stability advantage of aceclofenac salts. Cryst Growth Des. 2013;13(4):1590-601. doi: 10.1021/cg301825u.
4. Vadher AH, Parikh JR, Parikh RH, Solanki AB. Preparation and characterization of co-grinded mixtures of aceclofenac and neusilin US2 for dissolution enhancement of aceclofenac. AAPS PharmSciTech. 2009;10(2):606-14. doi: 10.1208/s12249-009-9221-6, PMID 19444620.

5. Tran P, Pyo YC, Kim DH, Lee SE, Kim JK, Park JS. Overview of the manufacturing methods of solid dispersion technology for improving the solubility of poorly water-soluble drugs and application to anticancer drugs. Pharmaceutics. 2019;11(3):132. doi: 10.3390/pharmaceutics11030132, PMID 30893899.
6. Luke DR, Tomaszewski K, Damle B, Schlamm HT. Review of the basic and clinical pharmacology of sulfobuty lether-β-cydodextrin (SBECD). J Pharm Sci. 2010;99(8):3291-301. doi: 10.1002/jps.22109, PMID 20213839.
7. Nurismi E, Rosaini H. Effect of different methods on the multi components crystal formation from medicinal natural ingredient compounds. Int J Pharm Sci Med. 2021;6(5):32-9. doi: 10.47760/ijpsm.2021.v06i05.004.
8. Grothe E, Meekes H, Vlieg E, ter Horst JH, de Gelder R. Solvates, salts, and cocrystals: a proposal for a feasible classification system. Cryst Growth Des. 2016;16(6):3237-43. doi: 10.1021/acs.cgd.6b00200.
9. Kumar S, Nanda A. Pharmaceutical cocrystals: an overview. Indian J Pharm Sci. 2017;79(6):858-71. doi: 10.4172/pharmaceutical-sciences.1000302.
10. Guo M, Sun X, Chen J, Cai T. Pharmaceutical cocrystals: a review of preparations, physicochemical properties and applications. Acta Pharm Sin B. 2021;11(8):2537-64. doi: 10.1016/j.apsb.2021.03.030, PMID 34522597.
11. Karimi Jafari M, Padrela L, Walker GM, Croker DM. Creating cocrystals: a review of pharmaceutical cocrystal preparation routes and applications. Cryst Growth Des. 2018;18(10):6370-87. doi: 10.1021/acs.cgd.8b00933.
12. Putri D. Review: multi-component crystals: cinnamic acid as a co-former. IJPSM. 2021;6(1):92-8. doi: 10.47760/ijpsm.2021.v06i01.008.
13. Afzal H, Abbas N, Hussain A, Latif S, Fatima K, Arshad MS. Physicomechanical, stability, and pharmacokinetic evaluation of aceclofenac dimethyl urea cocrystals. AAPS PharmSciTech. 2021;22(2):68. doi: 10.1208/s12249-021-01938-7, PMID 33564940.
14. Sharma G, Saini MK, Thakur K, Kapil N, Garg NK, Raza K. Aceclofenac cocrystal nanoliposomes for rheumatoid arthritis with better dermatokinetic attributes: a preclinical study. Nanomedicine (Lond). 2017;12(6):615-38. doi: 10.2217/nnm-2016-0405, PMID 28186461.
15. Kumar S, Gupta A, Prasad R, Singh S. Novel aceclofenac cocrystals with l-cystine: virtual coformer screening, mechanochemical synthesis, and physicochemical investigations. Curr Drug Deliv. 2021;18(1):88-100. doi: 10.2174/1567201817666200817110949, PMID 32807053.
16. Sohrab M, Mahapatra SP, Tiwari S. Enhancement of dissolution rate of aceclofenac by formation of aceclofenac-nicotinic acid cocrystal using water-soluble polymers like PVPK-30, HPMCE5, SSG and na-CMC. Indo Glob J Pharm Sci. 2015;05(3):154-70. doi: 10.35652/IGJPS.2015.01.
17. Yuliandra Y, Hutabarat LJ, Ardila R, Octavia MD, Zaini E. Enhancing solubility and antibacterial activity using multi-component crystals of trimethoprim and malic acid. Pharm Educ. 2021;21(2):296-304. doi: 10.46542/pe.2021.212.296304.
18. Nugrahani I, Jessica MA. Amino acids as the potential co-former for co-crystal development: a review. Molecules. 2021;26(11):3279. doi: 10.3390/molecules26113279, PMID 34071731.
19. Jelsch C, Devi RN, Noll BC, Guillot B, Samuel I, Aubert E. Aceclofenac and interactions analysis in the crystal and COX protein active site. J Mol Struct. 2020;1205:127600. doi: 10.1016/j.molstruc.2019.127600.
20. Vemuri VD, Lankalapalli S. Retracted: amino acid-based rosuvastatin cocrystals: towards the improvement of physicochemical parameters. J Cryst Growth. 2021;570:126241. doi: 10.1016/j.jcrysgro.2021.126241.
21. Rambabu D, Satyanarayana RJ, Saraswatula VG, Ravikumar N, Kamalakaran SA, Gopikrishna G. Novel cocrystals/molecular salts of mesalamine to be used as improved anti-inflammatory drug. 2012;A1:090224. Available from: https://www.freepatentsonline.com,WIPOPatentApplication2012/WO2012090224.html.
22. National Center for Biotechnology Information. PubChem compound summary for CID. Bethesda: National Library of Medicine (US). National Center for Biotechnology Information; 2022. p. 1117493.
23. Deters BJ, Saleem M. The role of glutamine in supporting gut health and neuropsychiatric factors. Food Sci Hum Wellness. 2021;10(2):149-54. doi: 10.1016/j.fshw.2021.02.003.
24. Shiek Abdul Kadhar Mohamed Ebrahim HR, Chungath TT, Sridhar K, Siram K, Elumalai M, Ranganathan H. Development and validation of a discriminative dissolution medium for a poorly soluble nutraceutical tetrahydrocurcumin. Turk J Pharm Sci. 2021;18(5):565-73. doi: 10.4274/tjps.galenos.2021.91145.
25. Wu D, Zhang B, Yao Q, Hou B, Zhou L, Xie C. Evaluation on cocrystal screening methods and synthesis of multicomponent crystals: a case study. Cryst Growth Des. 2021;21(8):4531-46. doi: 10.1021/acs.cgd.1c00415.
26. Jacobs A, Amombo Noa FM. Co-crystals and co-crystal hydrates of vanillic acid. CrystEngComm. 2015;17(1):98-106. doi: 10.1039/C4CE01795A.
27. Chadha R, Kuhad A, Arora P, Kishor S. Characterisation and evaluation of pharmaceutical solvates of atorvastatin calcium by thermoanalytical and spectroscopic studies. Chem Cent J. 2012;6(1):114. doi: 10.1186/1752-153X-6-114, PMID 23039933.
28. Acebedo Martinez FJ, Alarcon Payer C, Barrales Ruiz HM, Niclos Gutierrez J, Dominguez Martin A, Choquesillo Lazarte D. Towards the development of novel diclofenac multicomponent pharmaceutical solids. Crystals. 2022;12(8):1038. doi: 10.3390/cryst12081038.
29. Bazzo GC, Pezzini BR, Stulzer HK. Eutectic mixtures as an approach to enhance solubility, dissolution rate and oral bioavailability of poorly water-soluble drugs. Int J Pharm. 2020;588:119741. doi: 10.1016/j.ijpharm.2020.119741, PMID 32783978.
30. Alshaikh RA, Essa EA, El Maghraby GM. Eutexia for enhanced dissolution rate and anti-inflammatory activity of nonsteroidal anti-inflammatory agents: caffeine as a melting point modulator. Int J Pharm. 2019;563:395-405. doi: 10.1016/j.ijpharm.2019.04.024, PMID 30978486.
31. Yadav AV, Shete AS, Dabke AP, Kulkarni PV, Sakhare SS. Co-crystals: a novel approach to modify physicochemical properties of active pharmaceutical ingredients. Indian J Pharm Sci. 2009;71(4):359-70. doi: 10.4103/0250-474X.57283, PMID 20502540.
32. Bunaciu AA, Udriştioiu EG, Aboul Enein HY. X-ray diffraction: instrumentation and applications. Crit Rev Anal Chem. 2015;45(4):289-99. doi: 10.1080/10408347.2014.949616, PMID 25831472.
33. Fatimah S, Ragadhita R, Husaeni DFA, Nandiyanto ABD. How to calculate crystallite size from X-ray diffraction (XRD) using scherrer method. Asean J Sci Eng. 2021;2(1):65-76. doi: 10.17509/ajse.v2i1.37647.
34. Butreddy A, Almutairi M, Komanduri N, Bandari S, Zhang F, Repka MA. Multicomponent crystalline solid forms of aripiprazole produced via hot melt extrusion techniques: an exploratory study. J Drug Deliv Sci Technol. 2021;63:102529. doi: 10.1016/j.jddst.2021.102529, PMID 33959199.
35. Patel RD, Raval MK, Bagathariya AA, Sheth NR. Functionality improvement of nimesulide by eutectic formation with nicotinamide: exploration using temperature-composition phase diagram. Adv Powder Technol. 2019;30(5):961-73. doi: 10.1016/j.apt.2019.02.010.
36. Wicaksono Y, Setyawan D, Siswandono S. Formation of ketoprofen-malonic acid cocrystal by solvent evaporation method. Indones J Chem. 2017;17(2):161-6. doi: 10.22146/ijc.24884.
37. Oberoi LM, Alexander KS, Riga AT. Study of interaction between ibuprofen and nicotinamide using differential scanning calorimetry, spectroscopy, and microscopy and formulation of a fast-acting and possibly better ibuprofen suspension for osteoarthritis patients. J Pharm Sci. 2005;94(1):93-101. doi: 10.1002/jps.20223, PMID 15761933.
38. Emami S, Siahi Shadbad M, Barzegar Jalali M, Adibkia K. Characterizing eutectic mixtures of gliclazide with succinic acid prepared by electrospray deposition and liquid assisted

grinding methods. J Drug Deliv Sci Technol. 2018;45:101-9. doi: 10.1016/j.jddst.2018.03.006.

39. Shekunov BY, Chattopadhyay P, Tong HHY, Chow AHL. Particle size analysis in pharmaceutics: principles, methods and applications. Pharm Res. 2007;24(2):203-27. doi: 10.1007/s11095-006-9146-7, PMID 17191094.
40. Krithikadatta J, Valarmathi S. Research methodology in dentistry: part II-the relevance of statistics in research. J Conserv Dent. 2012;15(3):206-13. doi: 10.4103/0972-0707.97937, PMID 22876003.
41. Alshora DH, Ibrahim MA, Zayed G, Al Rwashed MA, Abou-Taleb HA, Ali MF. The role of sodium lauryl sulfate on formulation of directly compressed tablets containing simvastatin and aspirin: effect on drugs dissolution and gastric mucosa. Saudi Pharm J. 2022;30(5):635-45. doi: 10.1016/j.jsps.2022.02.006, PMID 35693440.